

ORIGINAL ARTICLE

Manipulation and detection of single nanoparticles and biomolecules by a photonic nanojet

Yu-Chao Li^{1,2}, Hong-Bao Xin¹, Hong-Xiang Lei², Lin-Lin Liu³, Yan-Ze Li⁴, Yao Zhang¹ and Bao-Jun Li¹

Optical methods to manipulate and detect nanoscale objects are highly desired in both nanomaterials and molecular biology fields. Optical tweezers have been used to manipulate objects that range in size from a few hundred nanometres to several micrometres. The emergence of near-field methods that overcome the diffraction limit has enabled the manipulation of objects below 100 nm. A highly free manipulation with signal-enhanced real-time detection, however, remains a challenge for single sub-100-nm nanoparticles or biomolecules. Here we show an approach that uses a photonic nanojet to perform the manipulation and detection of single sub-100-nm objects. With the photonic nanojet generated by a dielectric microlens bound to an optical fibre probe, three-dimensional manipulations were achieved for a single 85-nm fluorescent polystyrene nanoparticle as well as for a plasmid DNA molecule. Backscattering and fluorescent signals were detected with the enhancement factors up to $\sim 10^3$ and ~ 30 , respectively. The demonstrated approach provides a potentially powerful tool for nanostructure assembly, biosensing and single-biomolecule studies.

Light: Science & Applications (2016) 5, e16176; doi:10.1038/lsa.2016.176; published online 2 December 2016

Keywords: nanoparticles; optical detection; optical manipulation; single biomolecules

INTRODUCTION

With the initial design based on Ashkin's pioneering work¹, optical tweezers have become excellent tools for trapping and detecting small objects², promoting some significant advances in physical science and technology as well as cellular and molecular biology^{3,4}. When applied to the manipulation of sub-100-nm objects, such as Rayleigh nanoparticles and biomolecules, the trapping strength of optical tweezers becomes insufficient due to the fundamental limit imposed by laser beam diffraction⁵ and the dramatic disturbances caused by Brownian motion⁶. By tethering biomolecules to dielectric microbeads, optical tweezers can be used to manipulate the beads as handles to manipulate the molecules in some biomechanical studies^{7,8}. However, direct manipulation and detection that are completely based on light-matter interactions are highly desired for single biomolecules.

Recently, near-field methods for optical manipulation and detection have attracted a large amount of attentions^{9,10} because they can overcome the diffraction limit of optical tweezers based on free-space laser beams. By using nano-devices, such as plasmonic tweezers^{11–14}, slot waveguides¹⁵ and photonic crystal resonators¹⁶, optical intensity has been confined within a near-field region well below the diffraction limit, exerting a sufficiently strong force to manipulate the nano-objects. However, as all of the devices are based on different nano-structures, a fabrication process with considerably high accuracy and complexity is required. Furthermore, most nano-structures are fixed on substrates^{5,14}, which makes manipulating the objects in three dimensions difficult. The first three-dimensional manipulation of a

sub-100-nm dielectric nanoparticle was demonstrated by Berthelot *et al*¹³ with a scanning near-field plasmonic tweezer that was based on a bowtie nano-aperture. To the best of our knowledge, three-dimensional manipulation, which requires no nano-fabrication process and is valid for both single dielectric nanoparticles and biomolecules, has not been achieved. Moreover, a real-time detection of signals from the manipulated objects, which is greatly beneficial in nanomaterial characterization and biomolecular diagnostics, remains a challenge for single sub-100-nm nanoparticles or biomolecules due to the small size and low refractive index contrasting with the surrounding medium¹⁰. In this work, we demonstrate a near-field method that combines three-dimensional optical manipulation with signal-enhanced detection of single nanoparticles and biomolecules, avoiding the use of elaborate nanostructures or free-space laser systems. The technique makes use of a photonic nanojet, a sub-wavelength beam that results from the constructive interference of the optical field¹⁷, to manipulate the objects and enhance the backscattering and fluorescent signals of the targets. After firstly reported by Chen *et al*¹⁸, photonic nanojets have found applications in numerous fields^{19–22}. Some studies have shown that the backscattering, fluorescent and Raman scattering signals of nanoparticles can be significantly enhanced by the photonic nanojets^{17,18,23}. The strong optical confinement and signal enhancement properties of the photonic nanojets provide exciting new possibilities for optical manipulation and detection of single sub-100-nm nanoparticles or biomolecules.

¹Institute of Nanophotonics, Jinan University, Guangzhou 511443, China; ²State Key Laboratory of Optoelectronic Materials and Technologies, School of Materials Science and Engineering, Sun Yat-Sen University, Guangzhou 510275, China; ³State Key Laboratory of Microbial Technology, School of Life Sciences, Shandong University, Jinan 250100, China and ⁴National Engineering Research Centre for Beijing Biochip Technology, Beijing 102206, China
Correspondence: Y Zhang, Email: zhyao5@jnu.edu.cn; BJ Li, Email: baojunli@jnu.edu.cn

Received 30 December 2015; revised 30 May 2016; accepted 3 June 2016; accepted article preview online 7 June 2016

MATERIALS AND METHODS

Fabrication of the parabolic optical fibre probe

The parabolic optical fibre probe was fabricated via a flame-heating technique from a commercial single-mode optical fibre (connector type: FC/PC, core diameter: 9 μm , cladding diameter: 125 μm) (Corning Inc., New York, NY, USA). The buffer and polymer jacket of the fibre were stripped off with a fibre stripper to obtain a bare fibre of 1 cm in length and 125 μm in diameter. Before heating, the fibre was sheathed by a glass capillary to ensure the stability of the fibre probe. The bare fibre outside the capillary was then heated by the outer flame of an alcohol lamp at about 530 $^{\circ}\text{C}$ for 30 s to reach its melting point. The fibre was drawn with a speed of $\sim 2 \text{ mm s}^{-1}$ with a heating zone of $\sim 3 \text{ mm}$, and the fibre was gradually tapered off, with its diameter decreasing from 125 to 8 μm with a length of $\sim 1.6 \text{ mm}$. Finally, the drawing speed was increased up to $\sim 10 \text{ mm s}^{-1}$ until the fibre was broken with a parabolic tip.

Preparation of the particle suspension

The commercially available fluorescent polystyrene (PS) nanoparticles (Shanghai Huge Biotechnology Co., Ltd, Shanghai, China) have a refractive index of 1.58 and an emission at a 639-nm wavelength. The PS or titanium dioxide (TiO_2) microlenses and the fluorescent PS nanoparticles were first suspended in deionized water and then diluted to concentrations of $\sim 8.1 \times 10^3$ and $\sim 2.1 \times 10^4$ particles per μl , respectively. Then, equal weights of the PS or TiO_2 microlenses and the fluorescent nanoparticle suspensions were mixed together. The mixture of the PS or TiO_2 microlenses and the fluorescent PS nanoparticles was then dripped into the microfluidic chamber using a pipette for the following experiments.

Binding the microlens to the fibre probe

The PS or TiO_2 microlens was modified with aliphatic-amine and thereby became positively charged in such a way that they could bind to the surface of the negatively charged optical fibre probe in an aqueous environment. To align the microlens at the optical axis of the fibre probe, the microlens was firstly confined at the optical axis of the fibre probe by the optical gradient force, followed by moving the probe forward to touch the microlens. With this method, the deviation between the optical axis of the fibre and the microlens was suppressed below 250 nm.

Preparation of the plasmid DNA molecules suspension

The plasmid DNA molecules (3.4-kb long) were extracted from the *Escherichia Coli* strain DH5 α (Promega, Madison, WI, USA) using the Plasmid Mini Kit (Omega, Norcross, GA, USA) and kept in the elution buffer. The elution buffer consisted of 10 mM Tris-HCl at a pH of 8.5.

RESULTS AND DISCUSSION

Trapping strength of a photonic nanojet

To generate a photonic nanojet, we bound a dielectric microlens to an optical fibre probe via electrostatic attraction in an aqueous environment (Figure 1a). Both the illumination of the trapping light and the collection of detected signals were performed using the probe-microlens structure. The photonic nanojet, which was present on the shadowed side of the microlens, formed a potential well that trapped a nanoparticle near the microlens in a non-contact manner (inset of Figure 1a). To hold the microlens at the probe extremity and pre-focus the light, a parabolic fibre probe was fabricated by heating and drawing a single-mode optical fibre (see Materials and Methods). The diameter of the probe was decreased from 7.8 to 3.0 μm over a

length of 24.8 μm (Figure 1b). Optical fibre probes with parabolic or tapered shapes have been proposed for trapping micro-particles^{24–27}, but become insufficient when applied to the manipulation of sub-100-nm objects due to the fundamental diffraction limit. By modifying the charges in the probe and the microlens, the probe-microlens structure was stably bound and maintained in water (Figure 1c). To demonstrate observations with an optical microscope in the experiments, commercially available fluorescent PS nanoparticles with a diameter of $85 \pm 2 \text{ nm}$ (Figure 1d) were first used as an example of manipulated objects (see Materials and methods). When excited by a 398-nm laser, emission at 639 nm can be obtained from the fluorescent PS nanoparticles that can be observed with the optical microscope (Figure 1e). For a comparison of the trapping strength and signal enhancement, TiO_2 and PS microlenses with the same diameter (3 μm) were used to generate the photonic nanojets (Supplementary Fig. S1). The wavelength of the trapping light was 808 nm, which has the benefit of both generating smaller photonic nanojets than other commonly used trapping wavelengths, such as 1064 nm (Supplementary Fig. S2), and inducing little harm to the trapped objects, which is attributed to the low absorption by water or biological matter²⁸.

The trapping strength can be numerically investigated by performing three-dimensional simulations with a finite-element method (see details in Supplementary Information). The simulated electric field intensity distributions of the fibre probes indicate that the outputted beams were highly focused and formed into photonic nanojets, with distances of ~ 580 and $\sim 430 \text{ nm}$ in the x direction between the focuses of the nanojets and surfaces of the PS and TiO_2 microlenses, respectively (Figure 2a). Line scans were performed through the focal planes, and the results show that the full width at half maximum (FWHM) of the outputted light spots generated by the probe, PS microlens and TiO_2 microlens were 840, 385 and 208 nm, respectively (Figure 2b). The FWHM of the photonic nanojets of both the PS and TiO_2 microlenses were much smaller than the input wavelength (808 nm). To compare with the diffraction limit ($\sim 310 \text{ nm}$), the photonic nanojet was equivalent to a spherical light spot with the same effective volume. For example, the effective volume of the photonic nanojet generated by TiO_2 microlens was estimated from Figure 2b as $1.2 \times 10^7 \text{ nm}^3$, thus the diameter of the equivalent spot was $\sim 280 \text{ nm}$ which was smaller than the diffraction limit. With the photonic nanojets formed by the microlens, the probe-microlens structures provide a much stronger optical confinement than the bare probe (the insets in Figure 2b). In addition, the FWHM of the TiO_2 microlens was approximately two times smaller than that of the PS microlens because of the higher refractive index of TiO_2 ($n=1.99$) compared with that of PS ($n=1.58$). The optical force \mathbf{F}_O exerted on the PS nanoparticle, which was obtained by integrating the time-independent Maxwell stress tensor $\langle \mathbf{T}_M \rangle$ over the surface S enclosing the nanoparticle, can be expressed as²⁹

$$\mathbf{F}_O = \oint_S \langle \mathbf{T}_M \rangle \cdot \mathbf{n} dS \quad (1)$$

where \mathbf{n} is the surface normal vector. The optical force profiles were obtained for an 85-nm nanoparticle displaced in the x and y directions from the trapping regions (Figure 2c and 2d), with the focus position of the outputted light defined as the origin ($x=0.0$ and $y=0.0$) of the coordinate. By calculating the slopes near the trapping equilibrium position ($x=0.0$ or $y=0.0$) of the optical force curves (Figure 2c and 2d), the trap stiffness was then estimated as 0.06, 0.018 and 0.004 $\text{pN nm}^{-1} \text{ W}^{-1}$ in the x direction, while it was 0.31, 0.086 and 0.022 $\text{pN nm}^{-1} \text{ W}^{-1}$ in the y direction for the nanoparticle

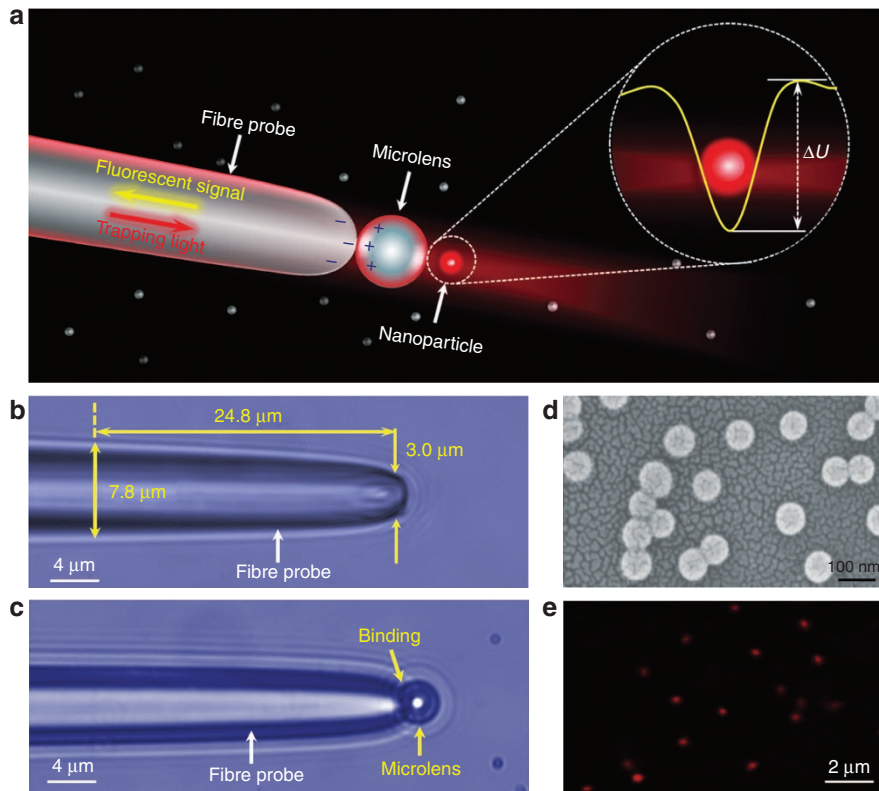


Figure 1 Experimental schematic illustration and images. **(a)** Schematic illustrating the manipulation and detection of a single nanoparticle by a photonic nanojet. The inset shows a nanoparticle trapped in a potential well formed by the photonic nanojet. The maximum potential difference is ΔU . **(b)** Optical microscope image of the probe used in the experiments. **(c)** Optical microscope image of the probe bound with a 3- μm microlens through electrostatic attraction. **(d)** Scanning electron microscope image of the fluorescent PS nanoparticles, with a diameter of 85 ± 2 nm. **(e)** Fluorescent image of the PS nanoparticles with a 639-nm emission excited by a 398-nm laser in the solution.

trapped by the probes with the TiO_2 microlens, PS microlens and without a microlens, respectively. Due to the stronger optical confinement, the trap stiffness in the y direction is ~ 5 times higher than that in the x direction. Accordingly, the corresponding radial trap stiffness (in the x - y plane) was estimated as 0.14, 0.039 and 0.009 $\text{pN nm}^{-1} \text{W}^{-1}$ for the nanoparticle trapped by the probes with the TiO_2 microlens, PS microlens and without a microlens, respectively. By integrating the x or y component (F_O) of \mathbf{F}_O over the distance D from the origin of the coordinate, the trapping potential U_O can be obtained according to

$$U_O = - \int F_O dD \quad (2)$$

The values of U_O were then obtained in both the x and y directions (Figure 2e and 2f). It can be seen that U_O reaches the minimum at $x=0.0$ and $y=0.0$, which indicates that the nanoparticle will be stably trapped on the focus of the outputted light. For the nanoparticle trapped by probes with the TiO_2 microlens, PS microlens and without a microlens, the potential differences ΔU_{x1} , ΔU_{x2} and ΔU_{x3} between the maximal and minimal points are 2.4×10^5 , 1.8×10^5 and 0.7×10^5 $k_B T/W$ in the x direction, while ΔU_{y1} , ΔU_{y2} and ΔU_{y3} are 5.0×10^5 , 4.2×10^5 and 1.5×10^5 $k_B T/W$ in the y direction, respectively. Thus, the photonic nanojet formed a three-dimensional potential well for the nanoscale objects. After the nanoparticles dropped into the potential well, they will be stably trapped in it until the energy related to the Brownian motion exceeds the maximum potential depth.

Manipulation of a nanoparticle

To trap the nanoparticles, the fibre probe was mounted on a six-axis microstage (resolution: 50 nm), with the parabolic end introduced into a microfluidic chamber that contained a solution of the microlens and nanoparticle mixtures (see detailed description of the experimental set-up in Supplementary Fig. S3). The other end of the fibre probe was connected to the stem of a 1:9 fibre coupler. The 808-nm laser beam was directly sent to the 10% arm of the coupler, while the 90% arm was connected to a photodetector with a bandpass filter (790–1200 nm) for detecting the reflected 808-nm signal. The 398-nm laser beam, launched into the other fibre with the end introduced into the solution, was used to excite the fluorescent nanoparticles. To monitor the binding process, a real-time trace of the reflected 808-nm signal R_1 was obtained (Figure 3a). The stable binding was indicated by an increased and steady signal R_1 . The probe-microlens structure (insets of Figure 3a) can be stably maintained and freely moved in three dimensions for subsequent manipulation of the nanoparticles or biomolecules (Supplementary Movie S1). By launching the laser beam into the fibre, a single 85-nm fluorescent PS nanoparticle was trapped by the photonic nanojet, and a real-time trace of the reflected signal R_2 was also performed for the trapping event (Figure 3b). Both the TiO_2 and PS microlenses could trap the particles and we present the results using the TiO_2 microlens in Figure 3b for the illustration. The optical power measured at the output of the probe-microlens was 3.2 mW, which allows the local intensity within the trap to be estimated as $1.2 \times 10^{10} \text{ W m}^{-2}$. Such an intensity is lower than that of conventional optical tweezers (typically

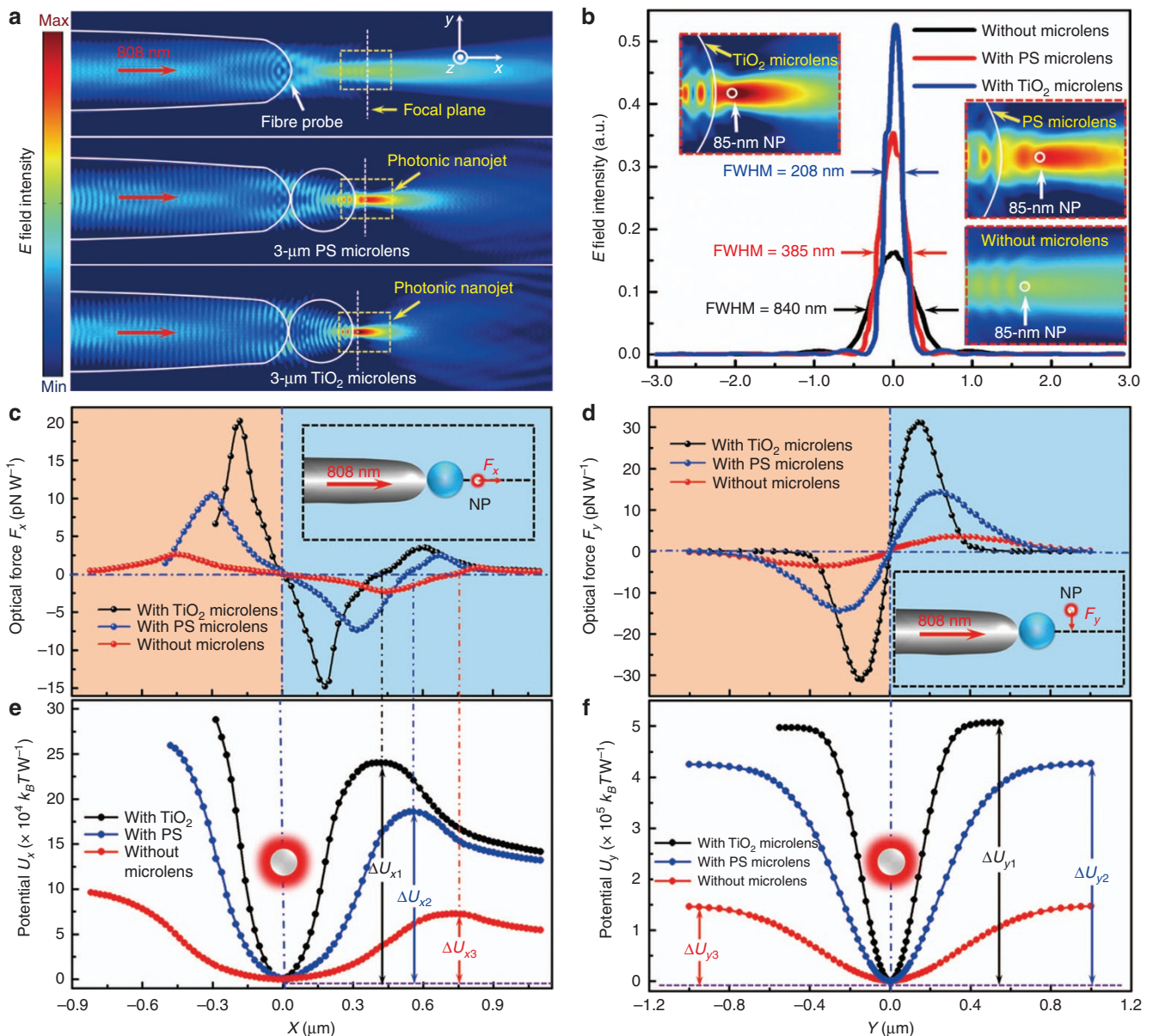


Figure 2 Trapping strength of the photonic nanojet. (a) Electric field intensity (E) distributions of probes without a microlens, with a 3- μm PS microlens and with a 3- μm TiO_2 microlens. An 85-nm PS nanoparticle (NP) is positioned at the focus of the outputted light. The red arrows show the 808-nm laser beam with an optical power of 1 W launched into the probe. (b) E field intensity at the focal planes of the outputted light in the y direction. The insets show the details of the focal regions of the outputted optical field in the dashed yellow regions of a. (c, d) Optical forces exerted on the NP along the optical axis of the probe as a function of the distance between the NP and the focus in the c x and d y directions. The insets show the calculation models. (e, f) Potentials as a function of the distance between the NP and the focus in the e x and f y directions.

from 1×10^{11} to 1×10^{12} W m^{-2}) and is compatible with biological matter. The real-time trace of R_2 shows three successive regimes: before the trapping (0–12.5 s), stable trapping (12.5–51.5 s) and releasing (51.5–64.7 s) of the single nanoparticle. The insets of Figure 3b show the corresponding optical microscope images of the trapping process. When the nanoparticle was trapped, the intensity of R_2 increases due to the backscattering light from the nanoparticle. In addition, the fluctuation of R_2 also increases due to the Brownian motion of the nanoparticle, which corresponds to the fluctuation of the distance between the trapped nanoparticle and microlens. The distance fluctuation of the nanoparticle during the trapping process exhibited a Gaussian distribution because of the Brownian motion of

the nanoparticle in a harmonic potential well. The central distance of the Gaussian fluctuation denoted the distance between the position of the trapped nanoparticle/DNA with the minimum potential (that is, the focus of the photonic nanojet) and the microlens. By statistically analysing the Gaussian fluctuation, the central distance can be obtained (see Supplementary Fig. S4 in the Supplementary Information). For example, the distance was calculated as ~ 480 nm for the nano-object trapped by the TiO_2 microlens (see Supplementary Fig. S4c and S4d), which agrees with the simulated distance of ~ 430 nm between the focus of the photonic nanojet and the microlens. These results confirmed that the nanoparticle was trapped in a non-contact manner.

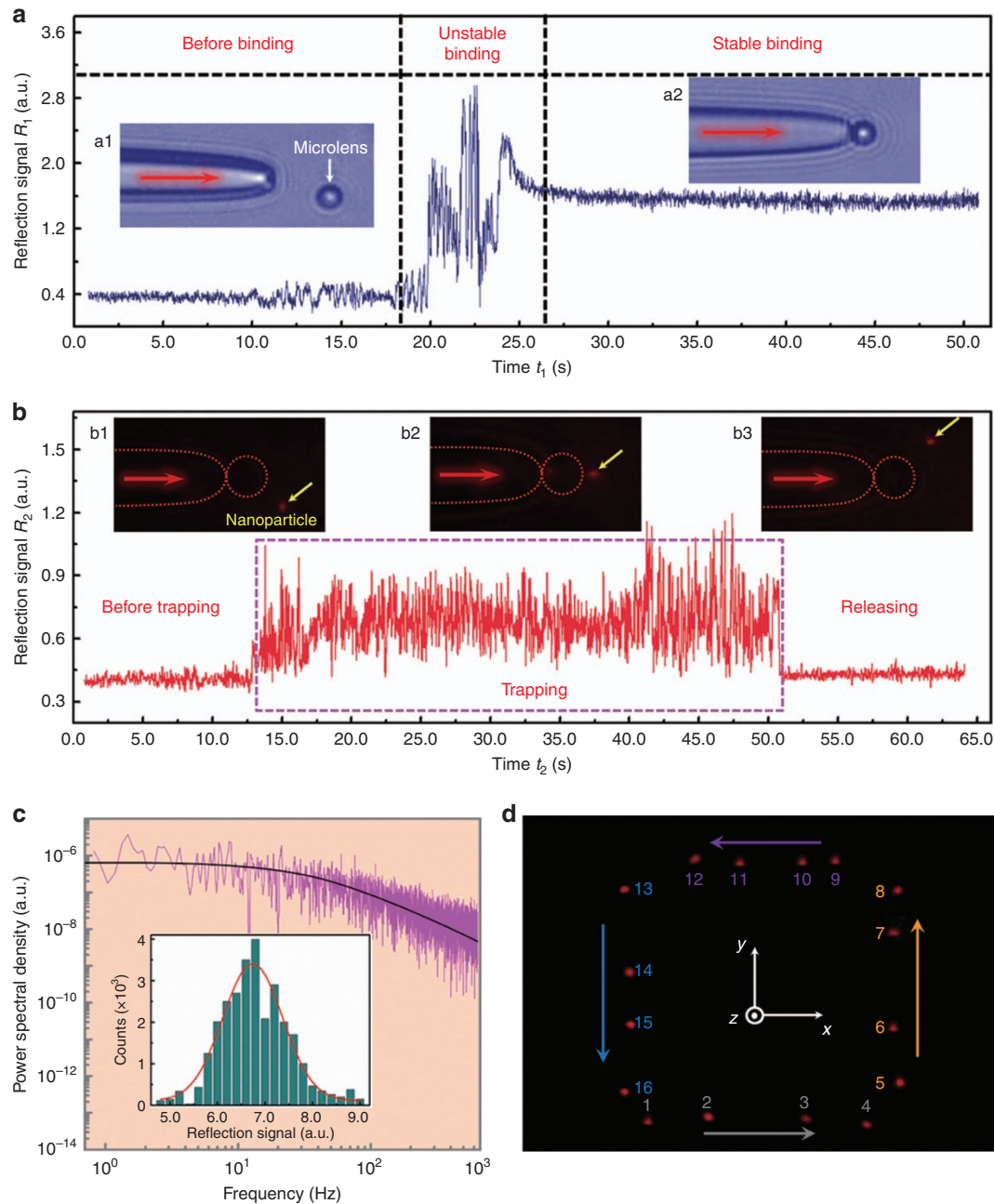


Figure 3 Manipulation and detection of a single 85-nm fluorescent PS nanoparticle. **(a)** Real-time trace of the reflected 808-nm signal R_1 in the microlens binding process. The signal was detected by the probe connected with a photodetector. The insets show optical microscope images **a1** without and **a2** with a 3- μm microlens bound to the probe. **(b)** The real-time trace of the reflected 808-nm signal R_2 in the trapping process of an 85-nm fluorescent PS nanoparticle. The insets show the fluorescent images **b1** before trapping, **b2** during trapping and **b3** in the release. **(c)** Power spectral density calculated from the data of R_2 in the trapping process and the fitted curve (black) to the Lorentzian model with a corner frequency of $f_c = 89.5$ Hz. The inset is the histogram calculated from the data of R_2 and the fitted curve (red) to the Gaussian model, which indicates that the nanoparticle was trapped in a harmonic potential. **(d)** Composite fluorescent image that shows the manipulation of the trapped nanoparticle in the x - y plane by controllably moving the probe in 24 s.

To quantify the trapping stiffness κ_{trap} in this system, a frequency-domain analysis was performed (Figure 3c), which considers the power spectral density of the nanoparticle's fluctuations in the trap^{30,31}. According to the results in Figure 3b, a histogram was obtained for the counts of R_2 from the trapping part, as shown by the inset of Figure 3c. The red full line is the Gaussian fit to the distribution, in which the central intensity is 6.7 in arbitrary units. The Gaussian distribution indicates that the nanoparticle dropped in a harmonic

trapping potential well and exerted a harmonic optical force: $F = -\kappa_{\text{trap}}x$, where x is the position of the nanoparticle relative to the trap centre. As shown in Figure 3c, the power spectrum of the nanoparticle fluctuation yields a Lorentzian function with a corner frequency of $f_c = 89.5$ Hz. As a result, the measured κ_{trap} was $0.13 \text{ pN nm}^{-1} \text{ W}^{-1}$ (see Supplementary Information for the frequency-domain analysis of the trapping stiffness), which is in agreement with the theoretical result ($0.14 \text{ pN nm}^{-1} \text{ W}^{-1}$). For a

comparison with the reported approaches, we scaled all of the κ_{trap} to an 85-nm particle, similar to those used in our experiments, because the optical force is proportional to the third power of the radius of the particle³². The κ_{trap} obtained by our approach was comparable to that of the slot waveguides¹⁵ (scaled $\kappa_{\text{trap}} = 0.12 \text{ pN nm}^{-1} \text{ W}^{-1}$) and two orders of magnitude higher than those of the conventional high numerical-aperture (NA) optical tweezers³³ (scaled $\kappa_{\text{trap}} = 0.0007 \text{ pN nm}^{-1} \text{ W}^{-1}$) and plasmonic tweezers¹⁴ (scaled $\kappa_{\text{trap}} = 0.001 \text{ pN nm}^{-1} \text{ W}^{-1}$).

After stably trapping, the nanoparticle was then manipulated in three dimensions by controllably moving the probe (Supplementary Movie S2). The moving trajectory was plotted by superimposing the microscope images that were captured at different instants with the same interval (Figure 3d). The nanoparticle was manipulated over a total distance of $\sim 60 \mu\text{m}$ in the x - y plane and $\sim 10 \mu\text{m}$ in the z direction. The ability to move a single nanoparticle to a desired position in three dimensions has benefits in nanomaterial science for the nanopatterning of the nanoparticles and the assembly of well-regulated nanostructures.

Signal enhancement in detection

When manipulating the nanoparticle, the fluorescent signal of the nanoparticle was also enhanced and detected by the microlens. In this case, the microlens acted as a high NA objective for collecting the signals. To determine the collection efficiency of the microlens, a three-dimensional finite-difference time-domain simulation (see details in Supplementary Information) was performed by placing a point source at 639 nm (the fluorescent wavelength) near the microlens (Figure 4a). The light from the source was collected by the probe-microlens structure with a collection angle of α . The effective numerical-aperture NA_{eff} was defined as $\text{NA}_{\text{eff}} = n \sin \alpha$, where

n is the refractive index of the microlens. The collection angle α and NA_{eff} were calculated as a function of the refractive index n of the microlens (Figure 4b), which indicates that the higher refractive index microlens has a greater collection efficiency. More specifically, the angles α of the PS and TiO_2 microlens were 42° and 59° , respectively, while the corresponding effective NA_{eff} were 1.10 and 1.71. Using the bare probe, the collection angles α and the effective NA_{eff} were 18° and 0.44, respectively, that is, a much lower collection efficiency compared with the PS and TiO_2 microlens. This finding is confirmed by the experiment that compared the detection of the fluorescent signals (Figure 4c–e). In the experiment, a fluorescent PS nanoparticle was trapped at the optical axis of the bare probe with a 3- μm distance to the tip. Without the microlens, the nanoparticle will be pushed away along the optical axis by the optical scattering force rather than attracted by the probe. To maintain the 3- μm distance between the nanoparticle and the probe, an opposite flow was employed to counteract the scattering force. The fluorescent signals were, respectively, collected by the bare probe (Figure 4c) and the probe-microlens structures (Figure 4d) and measured by an optical fibre spectrometer (integration time: 2 ms) with a bandpass filter (500–790 nm). The fluorescent spectra were obtained for the single nanoparticles that were detected by the bare probes without a microlens, with the PS microlens and the TiO_2 microlens (Figure 4e). In the presence of the PS and TiO_2 microlens, the fluorescent intensities of the nanoparticle were enhanced by factors of ~ 20 and ~ 30 , respectively.

Manipulation and detection of a plasmid DNA molecule

Compared with a dielectric nanoparticle, a single biomolecule is more difficult to manipulate or detect due to the lower refractive index, the smaller size and the irregular shape. We demonstrate that a single biomolecule can also be manipulated and detected by a photonic

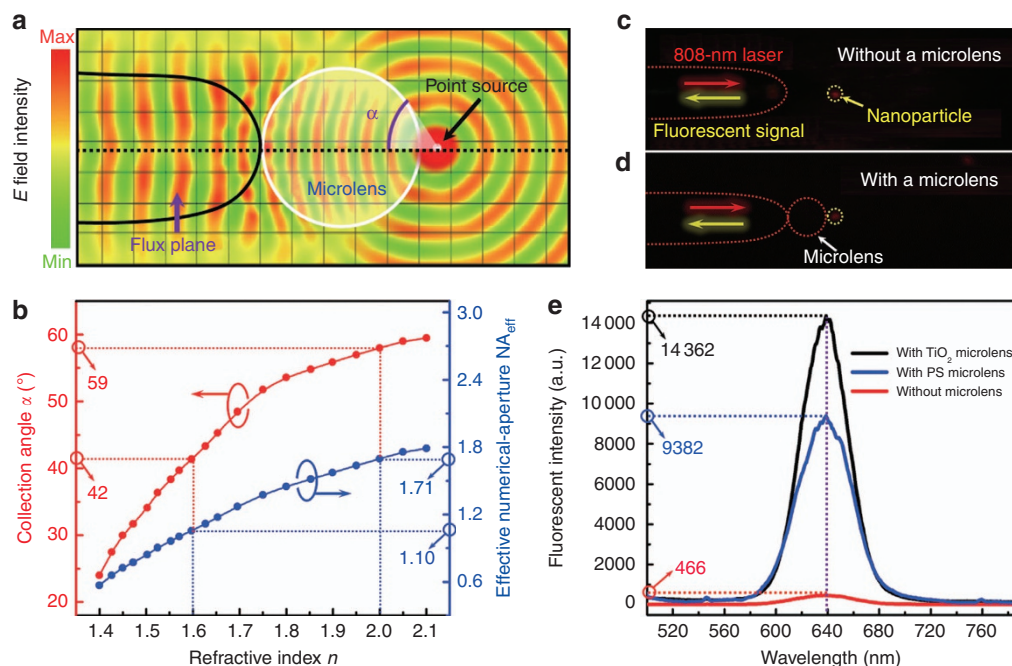


Figure 4 Signal enhancement by the probe-microlens structure. (a) Simulated E field intensity distribution. A point source was placed near the microlens. The light was collected by the probe-microlens structure with a collection angle of α . (b) Collection angle α and effective numerical-aperture NA_{eff} as a function of the refractive index n of the microlens. (c, d) Images of detecting the fluorescent signals of a single nanoparticle by the probes c without a microlens and d with a microlens. (e) Fluorescent intensities from the single nanoparticle detected by the probes without a microlens (red), with a 3- μm PS microlens (blue) and with a 3- μm TiO_2 microlens (black).

nanoscale. Plasmid DNA molecules (3.4-kb long) were used as an example of manipulated biomolecules (see Materials and methods). Before the trapping, the plasmid DNA molecules exhibited remarkable Brownian motion in the solution. By sending the 808-nm laser beam with a power of 5 mW ($1.9 \times 10^{10} \text{ W m}^{-2}$) into the fibre probe, a single DNA molecule was successfully trapped by the photonic nanoscale and then manipulated in three dimensions (Figure 5a–c; Supplementary Movies S3 and S4). In the experiment, the DNA molecules were illuminated in the transverse side by a 532-nm laser with an optical power of 150 μW . After the irradiation, the single DNA molecules were directly observed in the dark field by the scattering light (Figure 5d). Note that the trapped DNA molecule was less stable than the PS nanoparticles because the DNA molecules were in a partially extended state (as indicated by Figure 5d), which makes the trapping more difficult. The trapped DNA will eventually be released due to the increased Brownian motion and the fluctuations of the environment. We measured the average trapping time as a function of the optical power P (Figure 5e). The results show that at $P < 3 \text{ mW}$, the trapping events were not observed, while at $P > 3 \text{ mW}$, the

trapping time increased linearly with the power because of the increasing optical force and trapping potential. By utilizing the method mentioned above, the reflected signal R_3 of the trapped DNA was also detected to obtain a real-time trace in the trapping event (Figure 5f). The intensity of R_3 increases due to the backscattering light of the DNA when the trapping events occurred. The fluctuation of R_3 of the DNA was larger than that of the nanoparticle due to the stronger Brownian motion. In this case, the distance between the trapped DNA molecules and the microlens also exhibited a larger fluctuation so that the molecules would occasionally touch the microlens (see Supplementary Fig. S4e and S4f in the Supplementary Information). By increasing the optical power to 7 mW, the Brownian motion of the DNA molecules was efficiently suppressed due to the stronger optical forces so that the trapped DNA could hardly touch the microlens (Supplementary Fig. S4g and S4h).

Note that although the experimental set-up for illuminating the DNA was the same as that for exciting the fluorescent nanoparticles, we used the 532-nm light for illuminating the DNA rather than 398-nm light because such an illumination method can avoid the elaborate

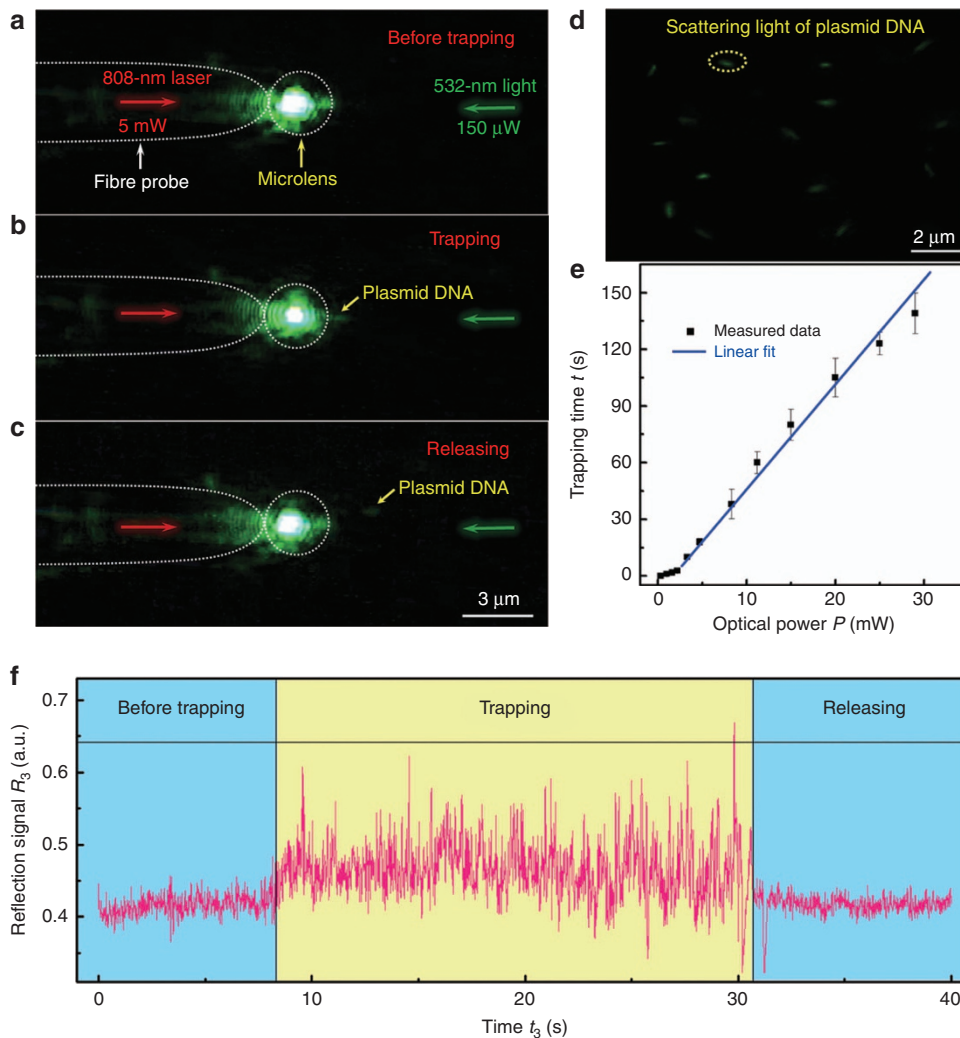


Figure 5 Manipulation and detection of a single plasmid DNA molecule. (a–c) Dark-field light-scattering images (a) before trapping, (b) during trapping and (c) in the release of a single plasmid DNA molecule. (d) The dark-field light-scattering image of the DNA molecules illuminated by the 532-nm light. The yellow dotted ellipse indicates the scattering light of a single DNA molecule. (e) Trapping time t as a function of the optical power P , with a linear fit applied to the measured data for $P \geq 3 \text{ mW}$. (f) Real-time trace of the reflected 808-nm signal in the trapping process of a DNA molecule.

process of labelling the DNA with the fluorophore and reduce the risk of photo-damages to the DNA caused by the ultraviolet exciting light (398 nm). However, the relatively strong scattering of the 532-nm light caused by the microlens partly affected the observation of the trapped DNA with the optical microscope (Figure 5a–5c). To reduce the scattering effects at the microlens, we alternated the illumination scheme by launching the illuminating light together with the trapping light into the fibre probe. Moreover, a laser beam with a shorter wavelength (473 nm) and lower power (10 μ W) was used as the illuminating light. With this method, the scattering at the microlens can be greatly reduced (see Supplementary Fig. S5 in the Supplementary Information).

In the simulations and calculations presented in previous sections, the photonic nanojet was generated by illuminating the microlens with a Gaussian beam through the fibre probe which was exactly aligned to the microlens. However, a misalignment between the optical axis of the optical fibre and the microlens may exist in the experiments. With a binding method, the misalignment can be suppressed below 250 nm (see Materials and methods). To investigate the influence of the misalignment on the optical trapping, additional simulations and calculations have been performed (see Supplementary Fig. S6 in Supplementary Information). The results show that although a misalignment of 250 nm between the fibre and microlens will slightly decrease the optical forces and potentials of the photonic nanojets, the decrement is very small so that the objects can also be trapped and manipulated under such a misalignment. Moreover, compared with the typical illumination condition using plane waves, the microlens illuminated by an optical fibre can pre-focus the light and generate a photonic nanojet with a smaller size and higher intensity, which provides stronger optical forces and larger potentials for trapping nanoparticles (see Supplementary Fig. S6 in Supplementary Information). It should be noted that besides the misalignment discussed above, the size and potentials of the photonic nanojets can also be affected by the distance between the microlens and fibre probe. In fact, it has been demonstrated that by re-positioning the microlens, a nanojet engineering in terms of size, trapping force and potential can be implemented in conventional optical tweezers²². In our approach, such an engineering can be realized by adjusting the laser power launched into the fibre probe. This is because the laser power will modulate the radiation pressure exerted on the microlens so that the microlens can be pushed away from the probe and then counter-balanced with the electrostatic attraction at a desired distance. This additional tuning of the nanojet will further extend the trapping and detection applicability.

In the experiments, the detection of a fluorescent signal was demonstrated as an example. Other signals, such as backscattering and Raman scattering signals, can also be enhanced and detected with the same method, which can find applications in super-resolution optical microscopy and single-molecule imaging^{19,23,34}. For example, additional simulations and calculations show that the backscattering signals of an 85-nm nanoparticle can be enhanced with factors of 1.5 and 5.3×10^3 in the photonic nanojets generated by the PS and TiO₂ microlenses, respectively (see Section 9 with Supplementary Fig. S7 in the Supplementary Information for the simulation and calculations of the backscattering enhancement).

It also should be noted that the optical manipulation of λ -DNA molecules (48-kb long) has been demonstrated by Yang *et al*¹⁵ with slot waveguides. However, the manipulation (transport along a straight path) was in two dimensions. Moreover, the optical power required for the slot waveguide approach was 200 mW, which is higher than that required for the demonstrated approach (5 mW). The lower level

of the optical power in the manipulation benefits in reducing the risk of damage to the DNA molecules, which is highly desired in single-molecule studies.

CONCLUSIONS

In summary, a near-field approach was proposed and demonstrated for realizing three-dimensional optical manipulation and detected signal enhancement of single sub-100-nm objects. The technique makes use of the photonic nanojet from the probe-microlens structure to generate a potential well that is strong enough to trap a single dielectric nanoparticle as well as a single biomolecule, at a relatively low optical power level. The 85-nm PS nanoparticles and plasmid DNA molecules were controllably manipulated in three dimensions over a long range, and the enhancement factors of the fluorescent and backscattering signals were up to ~ 30 and $\sim 10^3$, respectively. This technique requires no bulky optical elements or nano-fabrication processes, which liberates the manipulation and detection from free-space laser systems or nanostructures that are fixed on substrates. With the advantages of highly free manipulation, real-time detection, signal enhancement and low optical power consumption, the demonstrated approach is expected to open new opportunities in a wide variety of scientific fields. The ability to controllably manipulate a single dielectric nanoparticle could benefit nanomaterial science for the assembly of nanostructures. The fusion of optical manipulation and the detection of a single biomolecule could also provide powerful tools for the analysis of physical and chemical properties of nanomaterials or protein molecules in a non-invasive manner. The real-time signal-enhanced detection could find applications in biosensing of viruses, small bacteria and biomolecules.

CONFLICT OF INTEREST

The authors declare no conflict of interest.

ACKNOWLEDGEMENTS

We thank Jiye Wu, Xiaoshuai Liu and Juan Li from the School of Physics and Engineering, Sun Yat-Sen University for experimental assistance and Guoxuan Zhu from the School of Physics and Engineering, Sun Yat-Sen University for discussions about the simulations. This work was supported by the Program for Changjiang Scholars and Innovative Research Team in University (IRT13042) and the National Natural Science Foundation of China (No. 61205165).

- 1 Ashkin A, Dziedzic JM, Yamane T. Optical trapping and manipulation of single cells using infrared laser beams. *Nature* 1987; **330**: 769–771.
- 2 Grier DG. A revolution in optical manipulation. *Nature* 2003; **424**: 810–816.
- 3 Mitchem L, Reid JP. Optical manipulation and characterisation of aerosol particles using a single-beam gradient force optical trap. *Chem Soc Rev* 2008; **37**: 756–769.
- 4 Dholakia K, Čížmár T. Shaping the future of manipulation. *Nat Photon* 2011; **5**: 335–342.
- 5 Maragò OM, Jones PH, Gucciardi PG, Volpe G, Ferrari AC. Optical trapping and manipulation of nanostructures. *Nat Nanotechnol* 2013; **8**: 807–819.
- 6 Kang P, Serey X, Chen YF, Erickson D. Angular orientation of nanorods using nanophotonic tweezers. *Nano Lett* 2012; **12**: 6400–6407.
- 7 Fazal FM, Block SM. Optical tweezers study life under tension. *Nat Photon* 2011; **5**: 318–321.
- 8 Ma J, Bai L, Wang MD. Transcription under torsion. *Science* 2013; **340**: 1580–1583.
- 9 Erickson D, Serey X, Chen YF, Mandal S. Nanomanipulation using near field photonics. *Lab Chip* 2011; **11**: 995–1009.
- 10 He LN, Özdemir ŞK, Zhu JG, Kim W, Yang L. Detecting single viruses and nanoparticles using whispering gallery microlasers. *Nat Nanotechnol* 2011; **6**: 428–432.
- 11 Juan ML, Righini M, Quidant R. Plasmon nano-optical tweezers. *Nat Photon* 2011; **5**: 349–356.
- 12 Kotnala A, Gordon R. Quantification of high-efficiency trapping of nanoparticles in a double nanohole optical tweezer. *Nano Lett* 2014; **14**: 853–856.
- 13 Berthelot J, Aćimović SS, Juan ML, Kreuzer MP, Renger J *et al*. Three-dimensional manipulation with scanning near-field optical nanotweezers. *Nat Nanotechnol* 2014; **9**: 295–299.

- 14 Grigorenko AN, Roberts NW, Dickinson MR, Zhang Y. Nanometric optical tweezers based on nanostructured substrates. *Nat Photon* 2008; **2**: 365–370.
- 15 Yang AHJ, Moore SD, Schmidt BS, Klug M, Lipson M *et al*. Optical manipulation of nanoparticles and biomolecules in sub-wavelength slot waveguides. *Nature* 2009; **457**: 71–75.
- 16 Chen YF, Serey X, Sarkar R, Chen P, Erickson D. Controlled photonic manipulation of proteins and other nanomaterials. *Nano Lett* 2012; **12**: 1633–1637.
- 17 Yang H, Cornaglia M, Gijs MAM. Photonic nanojet array for fast detection of single nanoparticles in a flow. *Nano Lett* 2015; **15**: 1730–1735.
- 18 Chen ZG, Taflove A, Backman V. Photonic nanojet enhancement of backscattering of light by nanoparticles: a potential novel visible-light ultramicroscopy technique. *Opt Express* 2004; **12**: 1214–1220.
- 19 Wang ZB, Guo W, Li L, Luk'yanchuk B, Khan A *et al*. Optical virtual imaging at 50 nm lateral resolution with a white-light nanoscope. *Nat Commun* 2011; **2**: 218.
- 20 Mcleod E, Arnold CB. Subwavelength direct-write nanopatterning using optically trapped microspheres. *Nat Nanotechnol* 2008; **3**: 413–417.
- 21 Zhang XA, Elek J, Chang CH. Three-dimensional nanolithography using light scattering from colloidal particles. *ACS Nano* 2013; **7**: 6212–6218.
- 22 Neves AAR. Photonic nanojets in optical tweezers. *J Quant Spectrosc Radiat Transfer* 2015; **162**: 122–132.
- 23 Alessandri I, Bontempi N, Depero LE. Colloidal lenses as universal Raman scattering enhancers. *RSC Adv* 2014; **4**: 38152–38158.
- 24 Liu ZH, Guo CK, Yang J, Yuan LB. Tapered fibre optical tweezers for microscopic particle trapping: fabrication and application. *Opt Express* 2006; **14**: 12510–12516.
- 25 Xin HB, Xu R, Li BJ. Optical trapping, driving, and arrangement of particles using a tapered fibre probe. *Sci Rep* 2012; **2**: 818.
- 26 Li YC, Xin HB, Liu XS, Li BJ. Non-contact intracellular binding of chloroplasts in vivo. *Sci Rep* 2015; **5**: 10925.
- 27 Taguchi K, Okada J, Nomura Y, Tamura K. Three-dimensional optical trapping for cell isolation using tapered fibre probe by dynamic chemical etching. *J Phys Conf Ser* 2012; **352**: 012039.
- 28 Svoboda K, Block M. Biological applications of optical forces. *Annu Rev Biophys Biomolec Struct* 1994; **23**: 247–285.
- 29 Schmidt BS, Yang AHJ, Erickson D, Lipson M. Optofluidic trapping and transport on solid core waveguides within a microfluidic device. *Opt Express* 2007; **15**: 14322–14334.
- 30 Berg-Sørensen K, Flyvbjerg H. Power spectrum analysis for optical tweezers. *Rev Sci Instrum* 2004; **75**: 594–612.
- 31 Tolić-Nørrelykke SF, Schäffer E, Howard J, Pavone FS, Jülicher F *et al*. Calibration of optical tweezers with positional detection in the back focal plane. *Rev Sci Instrum* 2006; **77**: 103101.
- 32 Juan ML, Gordon R, Pang YJ, Eftekhari F, Quidant R. Self-induced back-action optical trapping of dielectric nanoparticles. *Nat Phys* 2009; **5**: 915–919.
- 33 Neuman KC, Block SM. Optical trapping. *Rev Sci Instrum* 2004; **75**: 2787–2809.
- 34 Schwartz JJ, Stavrakis S, Quake SR. Colloidal lenses allow high-temperature single-molecule imaging and improve fluorophore photostability. *Nat Nanotechnol* 2010; **5**: 127–132.



This work is licensed under a Creative Commons Attribution-NonCommercial-ShareAlike 4.0 International License. The images or other third party material in this article are included in the article's Creative Commons license, unless indicated otherwise in the credit line; if the material is not included under the Creative Commons license, users will need to obtain permission from the license holder to reproduce the material. To view a copy of this license, visit <http://creativecommons.org/licenses/by-nc-sa/4.0/>

© The Author(s) 2016

Supplementary Information for this article can be found on the *Light: Science & Applications*' website (<http://www.nature.com/lisa>).